Journal of Materials Processing Technology 212 (2012) 1157–1168

Contents lists available at SciVerse ScienceDirect

Journal of Materials Processing Technology

journal homepage: www.elsevier.com/locate/jmatprotec

The influence of multi-pass friction stir processing on the microstructural and mechanical properties of Aluminum Alloy 6082

Magdy M. El-Rayes[a,b,*,1], Ehab A. El-Danaf[a,b,2]

[a] Mechanical Engineering Department, College of Engineering, King Saud University, P.O. Box 800-11421, Riyadh, Saudi Arabia
[b] Center of Excellence for Research in Engineering Materials (CEREM), College of Engineering, King Saud University, Saudi Arabia

ARTICLE INFO

Article history:
Received 15 August 2011
Received in revised form
29 December 2011
Accepted 31 December 2011
Available online 8 January 2012

Keywords:
Friction stir processing
6082 Aluminum Alloy
Multi-pass friction stir processing
Dynamic recrystallization, Second phase particles

ABSTRACT

Samples with one through three passes with 100% overlap were created using friction stir processing (FSP) in order to locally modify the microstructural and mechanical properties of 6082-T6 Aluminum Alloy. A constant rotational speed and three different traverse speeds were used for processing. In this article, the microstructural properties in terms of grain structure and second phase particles distribution, and also the mechanical properties in terms of hardness and tensile strength of the processed zone were addressed with respect to the number of passes and traverse speeds. The parameter combination which resulted in highest ultimate tensile strength was further compared with additional two rotation speeds. FSP caused dynamic recrystallization of the stir zone leading to equiaxed grains with high angle grain boundaries which increased with increasing the number of passes. The accumulated heat accompanying multiple passes resulted in increase in the grain size, dissolution of precipitates and fragmentation of second phase particles. Increasing the traverse speed on the other hand did not affect the grain size, yet reduced the particles size as well as increased the particle area fraction. Hardness and tensile test results of the stir zone were in good agreement where increasing the number of passes caused softening and reduction of the ultimate tensile strength, whereas, increasing the traverse speed increased the strength and hardness. Increasing the tool rotational speed did not have a significant influence on particle mean diameter, ultimate tensile strength and hardness values of the stir zone, whereas, it caused an increase in mean grain size as well as particle area fraction.

1. Introduction

During the last two decades, severe plastic deformation (SPD) has been demonstrated as an effective approach to produce ultra-fine grain (UFG) materials. Extensive research has been carried out to develop SPD techniques and to establish processing parameters to produce UFG metals and alloys; especially Aluminum Alloys (AA), with more desirable properties as summarized by Mishra and Ma (2005). Among different SPD techniques, friction stir processing (FSP) and equal channel angular pressing (ECAP) have possessed the main focus of researchers. Compared to FSP, multi-pass ECAP is characterized by very low strain rates and requires at least 6–8 passes to achieve micro or UFG as summarized by Liu and Ma (2008). They also added that this technique produces limited shapes and also relatively small quantities of material and is difficult to scale up. FSP on the other hand, is essentially a local thermo-mechanical metal working process that changes the local properties without influencing the properties of the bulk material. This causes intense plastic deformation/strain and elevated temperatures in the processed zone, resulting in the generation of fine recrystallized grains via dynamic recrystallization (DRX) and break-up of constituent particles. Thus FSP creates microstructure containing fine grains with large grain boundary misorientations as concluded by Johannes et al. (2007) and high-angle grain boundaries, features that are important for enhanced mechanical properties as summarized by Mishra and Ma (2005). Nakata et al. (2006) have achieved an improvement in the mechanical properties due to the microstructural modification of an aluminum die casting alloy by multi-pass friction stir processing (MP-FSP), which is a solid-state microstructural modification technique using a frictional heat and stirring action.

FSP has been also applied by Johannes and Mishra (2007) to produce superplastic-fine-grained microstructures by creating staggered pass samples of 7075 aluminum. These samples were made with one through four passes under identical conditions. Materials processed by single as well as multiple pass

* Corresponding author. Tel.: +966 1 4679906, fax: +966 1 4676652.
E-mail address: melrayes@ksu.edu.sa (M.M. El-Rayes).
[1] On leave from Production Engineering Department- Faculty of Engineering-Alexandria University.
[2] On leave from Mechanical Design and Production Department- Faculty of Engineering- Cairo University.

0924-0136/$ – see front matter © 2012 Elsevier B.V. All rights reserved.
doi:10.1016/j.jmatprotec.2011.12.017

exhibited superplasticity across various testing temperatures and strain rates while the as received materials exhibited elongations up to 200%. This study demonstrated the effectiveness of multiple passes-friction stir processing in creating larger areas of material with superplastic properties. However, the largest elongations were observed for the single pass material. It has been also concluded that grain boundary sliding is the primary mechanism for superplastic deformation of multiple pass samples of 7075 AA.

Ma et al. (2006a,b) applied five-pass FSP (with 50% overlap) on cast Al–Si–Mg A356 alloy and it was found that overlapping FSP did not exert a significant effect on the size and distribution of the Si particles. The Si particles broken by FSP were uniformly distributed in the entire processed zones created by multiple-pass FSP. It was found that in the as-FSP condition, the strength and ductility of the transitional zones between two FSP passes were slightly lower than those of the nugget zones. Further, in the multiple-pass material the strength of the previously processed zones was lower than that of the subsequent processed zones due to overaging from the FSP thermal cycles. After T6-heat treatment the tensile properties of the 5-pass FSP A356 samples were similar across various passes and comparable to those of the single-pass FSP sample.

From the above review and in spite of the importance of 6xxx series AA to various industries a limited number of research work have been devoted to FSP of this series. However, an attempt has been made by Elangovan and Balasubramanian (2008) to understand the effect of tool pin profile and tool shoulder diameter on FSP zone formation in 6061 AA. Five different tool pin profiles (straight cylindrical, tapered cylindrical, threaded cylindrical, triangular and square) with three different shoulder diameters have been used to process the joints. From this investigation it is found that the square pin profiled tool and irrespective of shoulder diameter produced mechanically sound and metallurgically defect free welds compared to other tool pin profiles.

Woo et al. (2007) have studied the influence of the stirring pin and pressing tool shoulder on the microstructural softening occurring during FSP and subsequent natural aging behavior of 6061-T6 AA. In that work it was found that the microstructural softening has occurred mainly due the frictional heating from the tool shoulder during FSP. Furthermore, the reduction of the longitudinal residual strain profiles within the bead area was correlated to the microstructural softening. In general, the softening in the DRX and thermo-mechanically affected zones is related to the dissolution of fine needle-shape precipitates (β'') due to frictional heating, which reduced the microhardness from the 110 to 70 HV. Softening has also occurred in the HAZ which was similarly related to the dissolution of (β'') and the growth of coarse precipitate phase, which reduced the initial hardness to 60 HV.

As the need for strong, lightweight, high corrosion resistance, high thermal and electrical conductivity, hot and warm formability materials has steadily been increasing, there has also been a growing interest in Aluminum Alloys which posses such properties like that found in age-hardenable Al–Mg–Si alloy. This alloy is categorized under the 6xxx AA series, which is suitable for different structural applications, automotive and aircraft industries, due to their strong modification of strength induced by precipitation phenomena as reported by Fujda et al. (2008). Takeda et al. (1998) on the other hand studied the precipitation behavior of Al–Mg–Si alloy. It was found that the metastable β'' precipitates played a major role in improving the hardness more than β' does. The Al–Mg–Si alloys can be strengthened by the precipitation of the metastable precursors to the equilibrium β (Mg_2Si) phase as reported by Murayama et al. (1998), Murayama and Hono (1999) and Sha et al. (2003). An understanding of these precipitation mechanisms during artificial aging is critical for achieving optimal properties. A number of studies on the aging behavior of Al–Mg–Si alloys have been conducted in several publications. Miao and Laughlin (1999, 2000a,b) have summarized the precipitation sequence for the 6xxx Al–Mg–Si alloy as follows:

$$\alpha(\text{sss}) \rightarrow \text{GP zones} \rightarrow \beta''\text{needles} \rightarrow \beta'\text{rods} + \text{lath} - \text{like particles}$$

$$\rightarrow \beta + \text{Si(various morphologies)}$$

where α(sss) is the supersaturated solid solution and GP zones are spherical clusters having an unknown structure. The exact composition of the alloy and the casting condition will directly influence the volume fraction of intermetallic phases present as demonstrated by Kuijpers et al. (2003, 2005). These intermetallic phases have different unit cell structures, morphologies, stabilities and physical and mechanical properties as demonstrated by Miao and Laughlin (1999, 2000a,b).

Friction stir welding (FSW); the origin of FSP, has been frequently applied on 6xxx AA. Mroczka and Pietras (2009) used 6082 AA whereas Rodrigues et al. (2009) used 6016 and Sauvage et al. (2008) used 6061. They have reported the difficulty of achieving UFG structure due to the instability of second phase particles β" which leads to its dissolution and coarsening which ultimately leads to larger DRX grains.

The large particle size for almost all processing conditions, can lead to relatively larger dynamically recrystallized grains because of the less pinning effect that these particles exert.

In the present work, the influence of traverse speed and number of passes [100% overlapping] on the microstructural and mechanical properties of the processed SZ in commercial cold rolled 6082 AA is investigated. This includes the evaluation of the extent of grain refinement of the SZ and the microstructural modification as well as the size and distribution of the second phase particles. Room temperature tensile and microhardness tests are also conducted in order to evaluate the influence of traverse speed and number of passes on the strength of the processed SZ. In addition, the influence of the tool rotational speed on the microstructural and mechanical properties of the SZ will be further investigated. This will be achieved by selecting the tool traverse speed and number of passes combination which resulted in highest UTS and comparing it with higher rotational speeds.

2. Experimental procedure

Commercial 6082-T651 AA plates – 6 mm thick, 100 mm wide and 120 mm long with a nominal composition in wt.% 1.2 Si, 0.75 Mg, 0.79 Mn and 97.01 Al were used. A series of FSP runs were conducted perpendicular to the rolling direction at constant tool rotational speed of 850 rpm and varying the work piece traverse speed and also the number of FSP passes according to Table 1.

FSP was carried out perpendicular to the direction of rolling by applying one, two and three passes in an overlapping fashion as shown in Fig. 1.

The tool was manufactured from Mo–W tool steel with a flat shoulder of 15 mm diameter, and a concentric square pin with an

Table 1
Experimental parameters.

FSP – parameters combination N (rpm) – feed (mm/min)	850–90	850–140	850–224
Number of passes 100% overlap	One pass Two passes Three passes	One pass Two passes Three passes	One pass Two passes Three passes

Note: The FSP – parameter combination which results in highest ultimate tensile strength will be further compared with tool rotational speeds of 1070 and 1350 rpm.

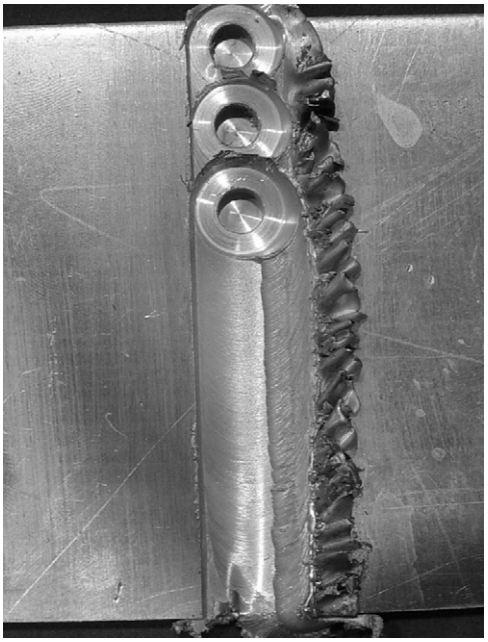

Fig. 1. FSP'ed sample using 3–100% overlapping passes.

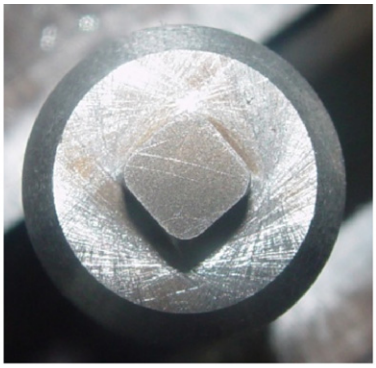

a)

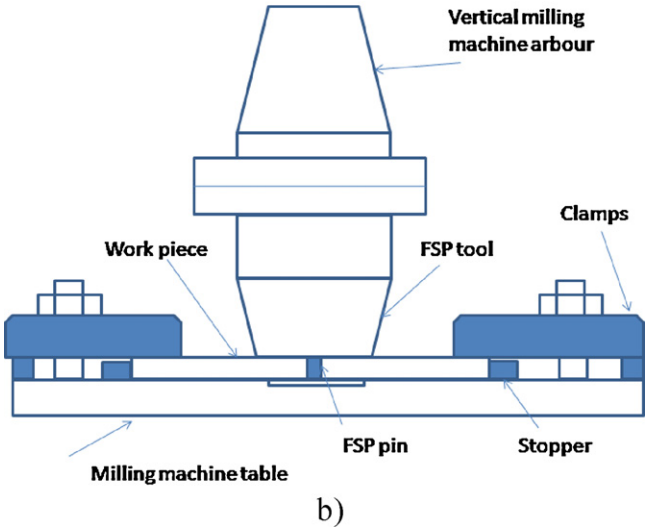

b)

Fig. 2. (a) FSP tool photo showing the tool shoulder and the square pin; (b) experimental set-up of FSP, El-Danaf et al. (2010).

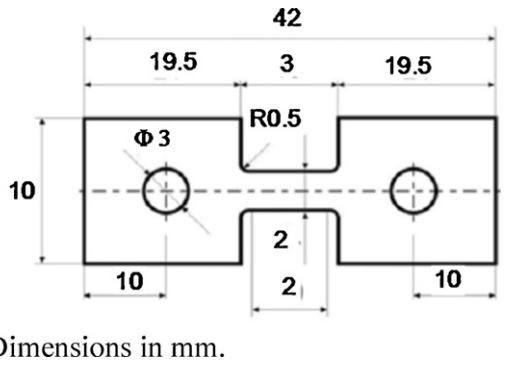

Dimensions in mm.

Fig. 3. Tensile test specimen.

edge length of 6 mm, and 5 mm long as shown in Fig. 2a). Test set-up which has been used in earlier work by El-Danaf et al. (2010) is shown schematically in Fig. 2b).

In order to reduce the extent of friction heating, cold air flow was directed during FSP towards the SZ. After processing the specimen was immediately immersed in cold water bath in order to hinder the growth of the dynamically recrystallized grains. Microstructure characterization was performed on all samples using optical microscope (OM). The microstructure of one sample was investigated by electron backscattered diffraction (EBSD). The FSP'ed specimens were prepared according to the standard procedures for specimen preparation including grinding, polishing and etching. Poulton's reagent was used to reveal the second phase particles and intermetallics, whereas, modified Poulton's reagent was used to reveal the specimen's microstructure; grain size, by immersion for 10 s. Grain size was measured by the linear intercept method and was further checked using "Buehler Omnimet" Image analyzer soft ware. The same software was also used to count the mean particle size and its density within the Aluminum matrix, where an average of five measurements was taken for each parameter. For EBSD, the sample was taken through the same procedure for OM, and further polished using colloidal silica on vibratory polisher. Microhardness measurements were taken on the specimen's cross section using Vickers microhardness testing using 300 g load and at 0.5 mm distance between successive indentations. In order to evaluate the mechanical behavior of FSP 6082 AA, miniature tensile specimens, shown in Fig. 3, were wire cut perpendicular to the FSP direction, with SZ being centered within the gage length.

For consistent results, it is worth noting that the microstructural characterization, microhardness measurements and also the extraction of tensile samples were conducted at a plane located 2.0 mm below the top of the SZ. Tensile samples were subsequently ground and polished to a final thickness of 2.0 mm. Room temperature tensile tests were conducted using a computer-controlled Instron machine model 3385 H, at a cross head speed of 2 mm/min. After testing, final length of failed specimens was measured to determine ductility.

3. Results and discussion

3.1. Microstructural characteristics of the processed region

The FSP runs were conducted in the direction perpendicular to the rolling direction having the microstructure shown in Fig. 4 in the as-received condition. Second phase particles are seen within the entire base metal microstructure. The average aspect ratio of the elongated grains was measured to be 2.1 by using image analyzer soft ware.

To document the grain structure and the distribution of second phase particles, optical microscopy was conducted on the SZ of

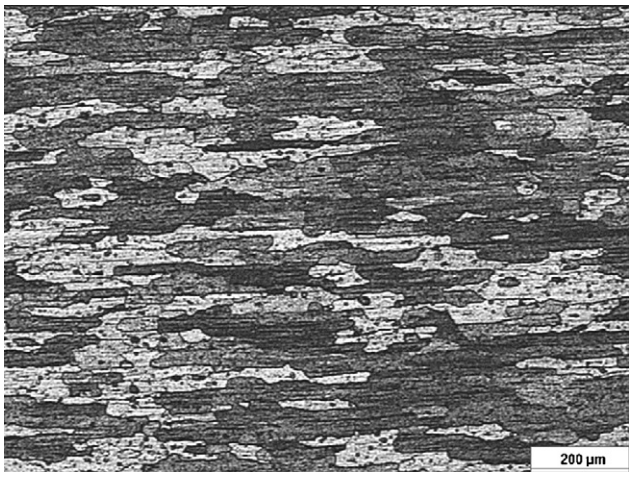

Fig. 4. Microstructure of the as-received Aluminum Alloy 6082-T651 base metal.

all processed samples. Orientation image microscopy (OIM) using electron back scattered diffraction on a Joel SEM analyzed and controlled by TSL software was employed on several samples.

The grain tolerance angle (GTA) embedded in the analysis was set as 15°, which means that boundaries are not defined unless the critical misorientation between two neighboring points is more than 15°, this was chosen with the purpose to define the grain structure of well defined grain boundaries. The two microscopy techniques were performed to validate the microstructure inferred for same processing conditions and to get information about the average misorientation angle developing through the OIM technique. Fig. 5(a)–(c) shows the image quality map, distribution of grain size and a histogram for the misorientation angle, respectively, for the sample processed at 850 rpm–90 mm/min for one pass, from the EBSD results. Fig. 5(d) shows the optical micrograph for the same sample. The average grain size and average misorientation angle, from EBSD, were depicted on the respective figure sections Fig. 5(b) and (c). The grain structure in the SZ, inferred from both microscopy techniques, attains the equiaxed morphology that has developed through dynamic recrystallization (DRX). Within this zone, severe plastic deformation and frictional heating occur during FSP resulting in the generation of a recrystallized

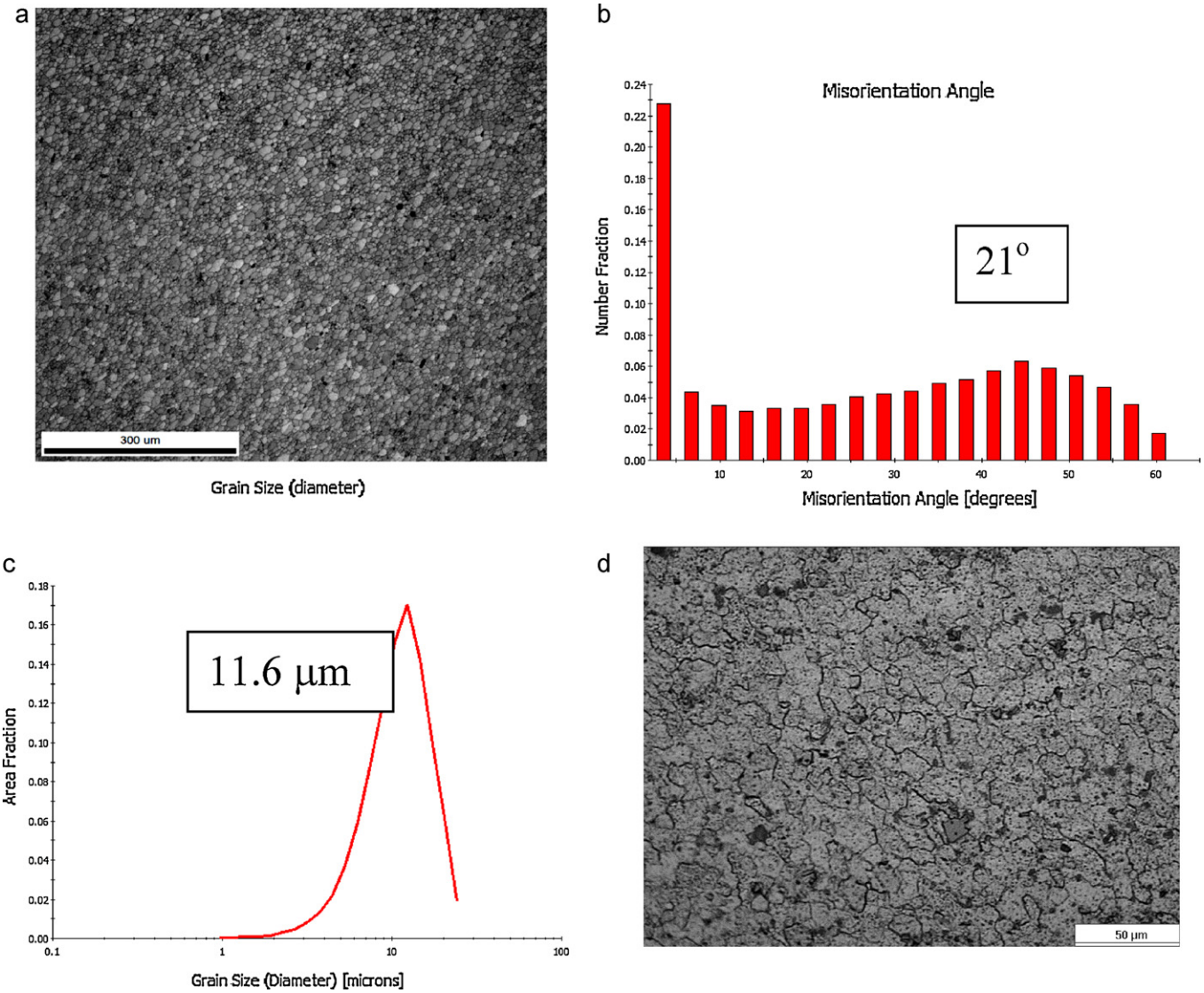

Fig. 5. EBSD results of a sample processed at 850 rpm, 140 mm/min using one passes. (a) Image quality map; (b) distribution of grain size; (c) histogram for the distribution of misorientation angle; (d) optical micrograph of SZ.

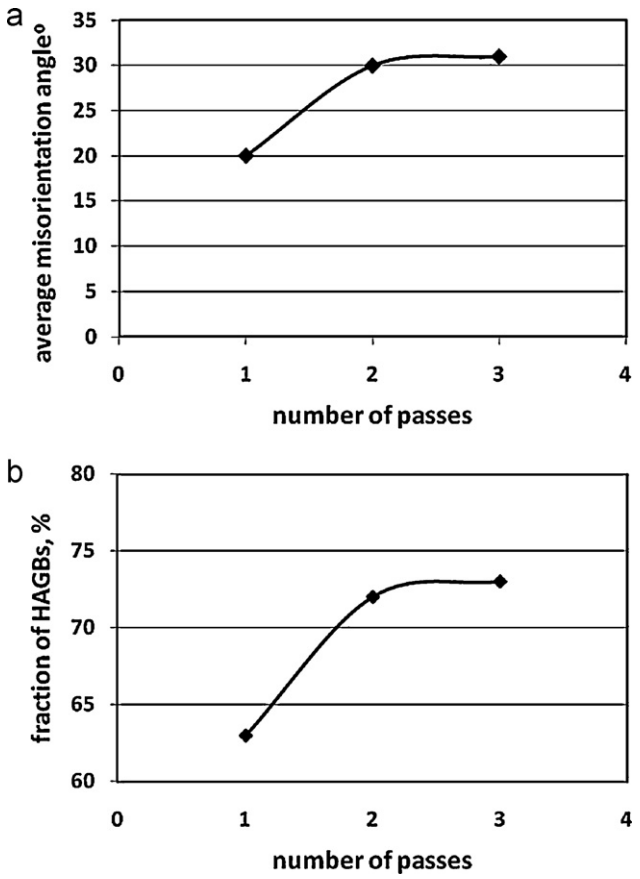

Fig. 6. The influence of varying number of passes on: (a) average misorientation angle; (b) fraction of high angle grain boundaries (HAGBs).

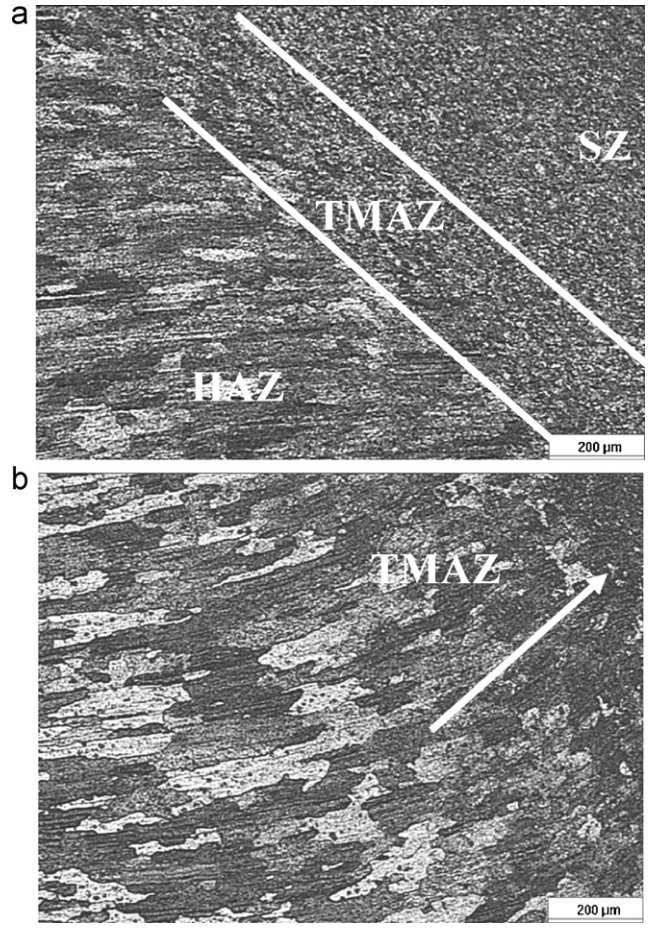

Fig. 7. (a) Transition between the SZ, TMAZ and HAZ; (b) partial recrystallization of grains [arrow] occurring at TMAZ on the retreating side.

fine-grained microstructure due to DRX. This result confirms with that reported earlier by Mishra and Ma (2005) and also by Mroczka and Pietras (2009). The grain size obtained, by linear intercept method; from optical microscopy was about 11.8 μm. It is obvious the close agreement of grain size calculated by both techniques.

Fig. 6(a) and (b) presents the evolution of average misorientation angle and fraction of high angle grain boundaries (HAGBs) with number of passes for the 850 rpm–224 mm/min processing condition. For all number of passes the average misorientation is relatively high, yet increasing with number of passes. Also, the fraction of HAGBs is seen to increase with number of passes, which shows that almost 73% of the boundaries, for the sample processed with three passes, are well developed true grain boundaries. This gives indication to the extent of DRX happening with increasing number of passes.

The thermo-mechanical affected zone (TMAZ), on the other hand, is found in the close vicinity of SZ, as shown in Fig. 7(a), where the material experiences lesser strains and strain rates as well as lower peak temperatures compared to the SZ. The TMAZ is characterized by a less deformed structure, in which the parent metal-elongated grains are markedly bent due to plastic deformation into the direction inclined to the TMAZ/SZ boundary, as in Fig. 7(a). A similar microstructure has been obtained by Scialpi et al. (2007). Although the TMAZ underwent plastic deformation, recrystallization did not fully occur in this zone due to insufficient deformation strain as reported by McNelley et al. (2008). The structure on the right in Fig. 7(b) [shown by arrow] appears to be partially recrystallized where some equiaxed grains started to form within the elongated-deformed grains. This structure has been found in all the FSP literature related to Aluminum Alloys.

The heat affected zone (HAZ) beyond the TMAZ, shown in Fig. 7(a), is a zone which experiences a thermal cycle, but does not undergo any plastic deformation and still retains the same grain structure as the parent material as documented earlier in several publications by Mishra and Ma (2005), Scialpi et al. (2007) and Adamowski and Szkodo (2007).

Fig. 8(a) and (b) shows the influence of varying the number of passes and traverse speeds on the SZ mean grain size respectively. Increasing the number of passes at a given traverse speed, causes an increase in the grain size, Fig. 8(a). This is due to the grain coarsening resulting from the additional/accumulated thermal cycles which the plate has experienced and the simultaneous occurrence of continuous dynamic recrystallization (CDRX) occurring with each FSP pass. This result is in good agreement with earlier work of Johannes and Mishra (2007). The increase in grain size is obvious between the second and third pass, whereas, between the first and second passes the increase is marginal.

On the other hand, increasing the traverse speed, at a given number of passes, slightly increases the grain size especially with first and second passes, whereas with third the pass almost no difference is noted, Fig. 8(b). It can therefore be stated that the traverse speed does not appear to be contributing to change the size of dynamically recrystallized grain in the SZ. The work done by Ma et al. (2006a,b) confirms this statement.

3.2. Second phase particles/intermetallic phases

AA 6xxx contain a large amount of various intermetallic particles with size typically ranging between 1 and 10 μm. Most of

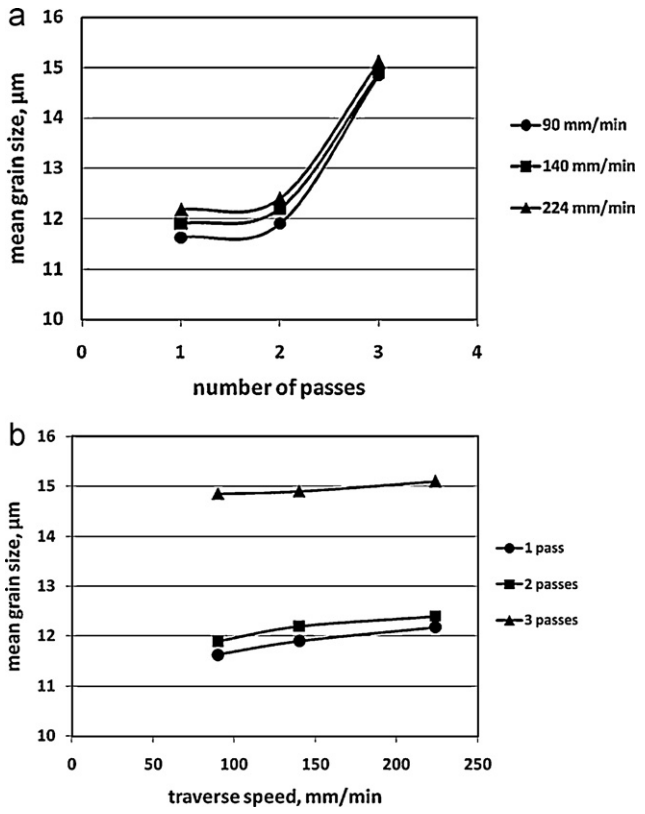

Fig. 8. Variation of grain size with: (a) number of passes; (b) traverse speeds.

the second phase particles were identified by energy dispersive X-ray spectroscopy (EDS) and X-ray diffraction (XRD), as typical Aluminum intermetallic phases containing Fe, Mn, Si and Mg. Fig. 9 shows the XRD pattern of the sample processed at 850 rpm–224 mm/min using three passes. Different intermetallic phases are identified and noted on their respective peaks.

Al–Mg–Si alloys can be strengthened through the precipitation of the metastable precursors of the equilibrium β (Mg_2Si) phase. As artificial aging commences, coherent needle-shaped β″ particles are precipitated leading to an increase in hardness. Urreta et al. (2001) showed that when the β″ needles are still thin (under aged condition), they are sheared or cut by glide dislocations. As aging continues these needles gradually grow and further harden the material, as many of the larger β″ precipitates behave as impenetrable obstacles. This is particularly the case at the beginning of plasticity in the peak-aged condition. In addition, Urreta et al. (2001) showed that the formation of the β″ hardening phase is a thermally activated process. As the aging process continues past the peak-aged condition, the β″ phase is reverted to larger, semi-coherent rod-like or lath-like β′ particles, resulting in a softening of the material.

At the final aging stage, equilibrium non-coherent Mg_2Si and silicon particles are precipitated. In this over-aged condition, precipitates are largely bypassed by dislocations through the Orowan mechanism. The low strength of over-aged samples is due to the poor solid solution hardening as the majority of the magnesium and silicon present in the alloy is precipitated as relatively large Mg_2Si or silicon particles. Unfortunately the β" precipitates are not temperature resistant and rapidly dissolve. In the SZ, due to the dramatic increase of the temperature, β″ precipitates partially dissolve and the rest coarsens to semi-coherent β′ and non-coherent equilibrium β precipitates. One should note that dislocations shearing and cutting precipitates may promote the decomposition of β″ giving rise to local super saturated solid solutions, which can give a dramatic loss of hardness in the weld nugget. A re-precipiation stage following the full decomposition of precipitates was proposed by Cabibbo et al. (2007) for a friction stir welded 6056 AA. However, considering the work of Frigaard et al. (2001) on a 6082 AA processed by FSW (T6 state, 1500 rpm, 300 mm/min), the temperature in the weld nugget is in a range of 350–480 °C during only 2 s. During this short time, few precipitates may survive and then coarsen during the cooling time as reported by Kamp et al. (2006).

Metallographic testing has revealed abundant amounts of second phase particles within the entire FSP'ed samples having different shapes, sizes and distributions. Fig. 10 shows a typical example of these particles at low magnification. Within the SZ, and due to the intensified stirring action, the second phase particles are homogeneously dispersed and have almost regular size, whereas, on the TMAZ side the particles size is heterogeneous ranging between coarse to fine particles. In addition, the density of particles within the TMAZ is obviously less than that in the SZ. This is inferred from the larger area of the aluminum matrix in this region.

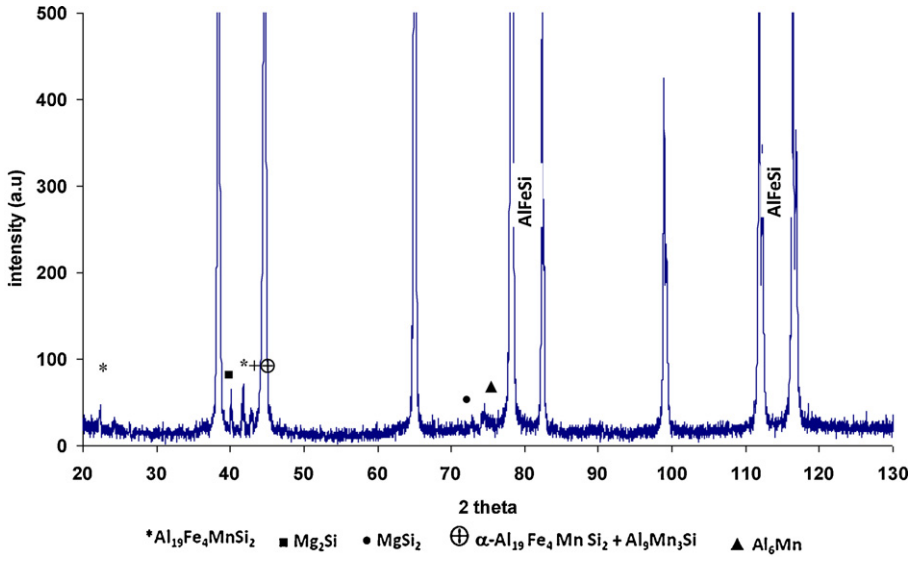

Fig. 9. XRD pattern of the SZ processed at 850 rpm-224 mm/min using three passes.

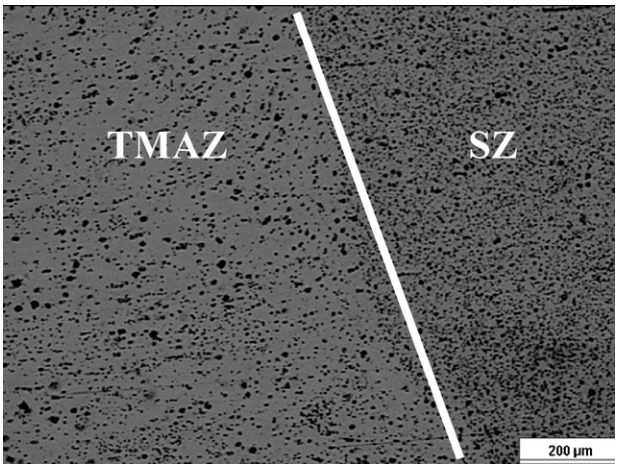

Fig. 10. Second phase distribution at the transition zone between SZ and TMAZ.

Fig. 11(a)–(c) shows, at higher magnification, the variation of size and distribution of these particles in the base metal, SZ and TMAZ respectively, for the sample processed under 850 rpm–90 mm/min using three passes. Coarse particles with various shapes and size are spread heterogeneously within the base metal as shown in Fig. 11(a). Within the SZ, the stirring action and the severe plastic deformation involved, which can lead to fragmentation, as well as decomposition and re-precipitation hypothesis mentioned-above, have resulted into smaller particles with occasional finer ones which possessed new locations. These particles are homogeneously dispersed throughout the matrix and have higher density, as shown in Fig. 11(b). The TMAZ on the other hand, is composed of few coarse particles and also clusters of fine particles which have formed in upward flow lines, as shown in Fig. 11(c).

Fig. 12(a) and (b) shows the influence of varying the number of passes at different traverse speeds on the particle area fraction and the particle mean diameter respectively. These parameters were obtained using image analyzer software. The particle area fraction represents the fraction of the matrix covered by second phase particles, i.e. density. The particle mean diameter refer to the average particle size. Increasing the number of passes as well as the traverse speed increases the density of second phase particles and simultaneously reduces the average particle size. These two inseparable particle features are inversely related as shown in Fig. 13, where the particle density is plotted against the particle size. The increased number of passes causes repetitive stirring action and more efficient mixing of plasticized SZ material; Mironov et al. (2008), which leads to more fragmentation and re-precipitation of new particles thus occupying a larger area with respect to the matrix, as in Fig. 12(a). This fragmentation consequently causes more particle refinement, as per Nakata et al. (2006), which is expressed in smaller particle diameter as shown in Fig. 12(b). A probable reason, for the increased particle density/reduced particle size with number of passes, is due to the increased tendency of precipitate nucleation. Rodrigues et al. (2009) have reported that precipitates nucleate randomly at dislocations and the extent of nucleation is strongly dependant on the dislocation density, which makes highly plasticized SZ materials suitable for nucleating precipitates.

On the other hand, increasing the traverse speed at constant number of passes slightly increases the density of second phase particles, Fig. 12(a), and simultaneously reduces the mean particle size, as in Fig. 12(b).

Jayaraman et al. (2010) have reported that increasing the traverse speed intensifies the movement of the stirred material from front to back of the pin; i.e. stirring action, thus promotes mixing of plasticized material. This favors the precipitates to

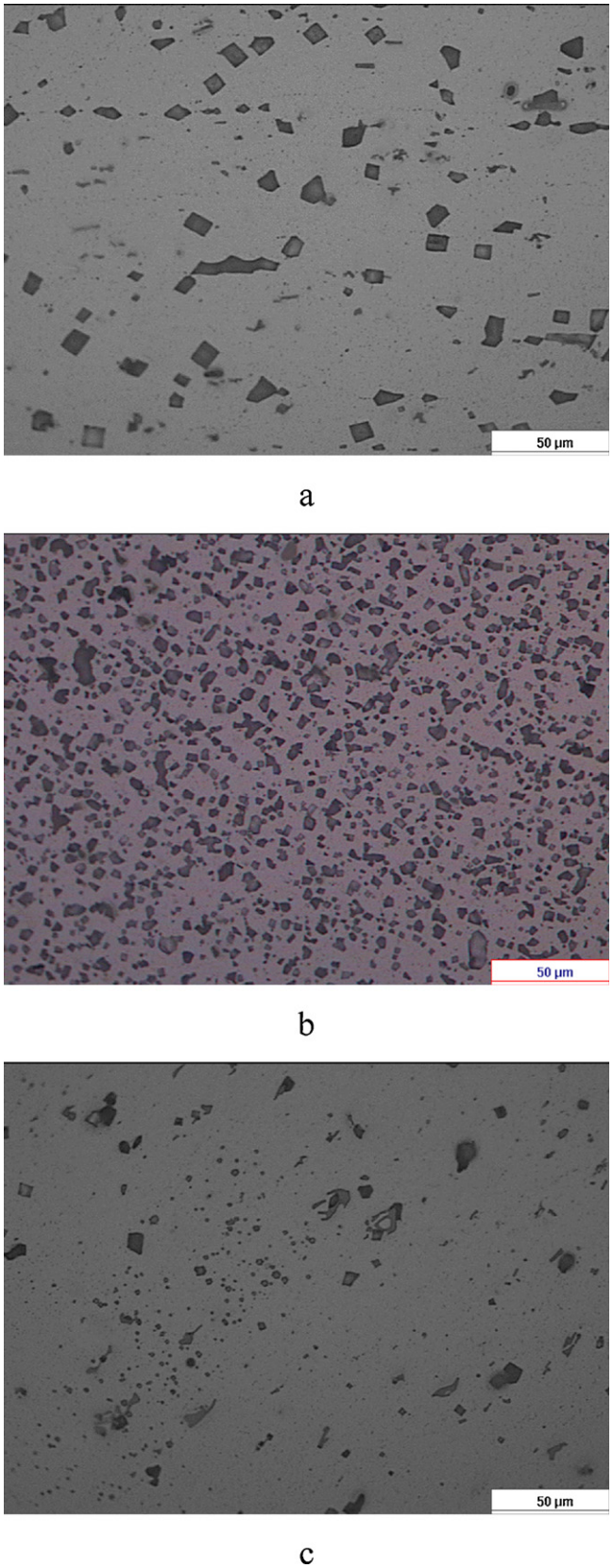

Fig. 11. Second phase particles found in specimen processed at 850 rpm, 90 mm/min using one pass taken at different locations: (a) base metal, (b) SZ and (c) TMAZ.

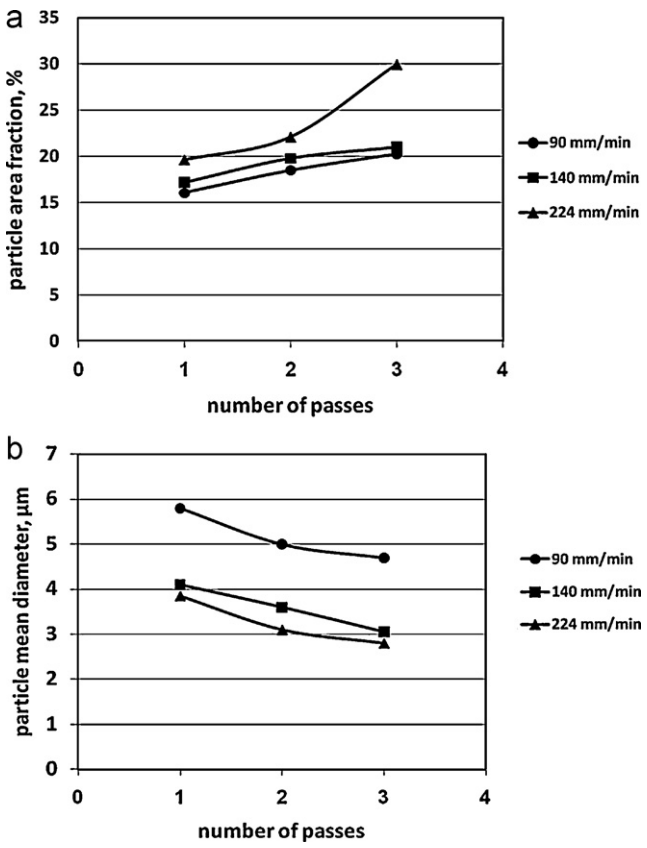

Fig. 12. Influence of number of passes on: (a) particle area fraction with respect to matrix, and (b) particle mean diameter.

nucleate at dislocations leading to an increase of the precipitates density, Fig. 11(a). Since the tool rotational speed was kept constant, therefore, increasing the traverse speed will cause an increase in the stirring influence per one revolution and consequently more fragmentation. Thus, leading to more distribution; i.e. higher density, and less particle size. The stirring influence per revolution have been calculated by converting traverse speed units from mm/min to mm/rev. [90 mm/min = 0.105 mm/rev.; 140 mm/min = 0.164 mm/rev.; 224 mm/min = 0.263 mm/rev.]. Also, it is expected that low traverse speed results into relatively more prolonged exposure to heating and consequently leads to coarser particles; shown in Fig. 12(b) as concluded by Jayaraman et al. (2010).

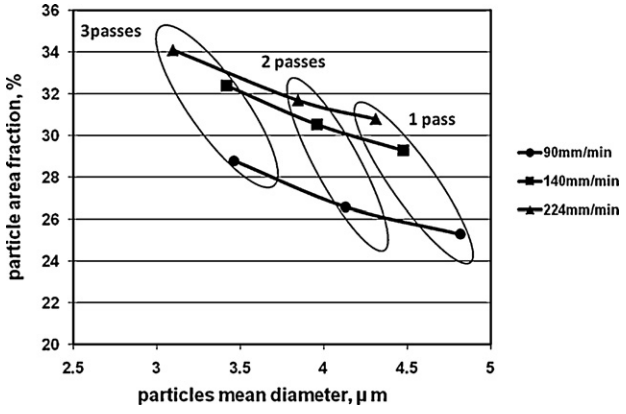

Fig. 13. Relation between particle area fraction vs. particle mean diameter at different traverse speeds and number of passes.

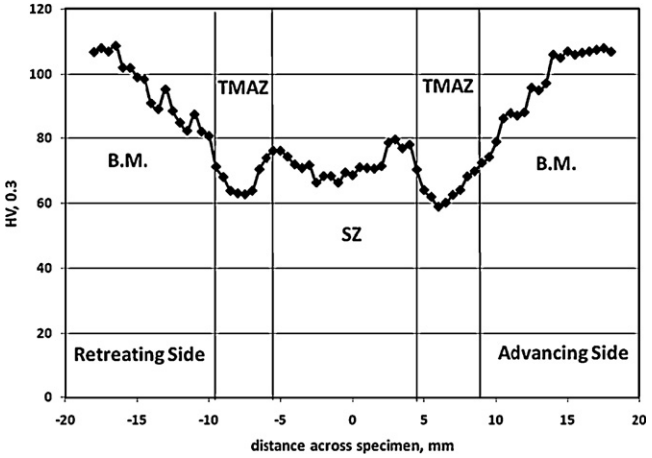

Fig. 14. Hardness distribution across FSP-ed specimen at 850 rpm and 140 mm/min using two passes. *Note*: advancing side is on the right of SZ, whereas, the retreating side is on the left.

3.3. Mechanical characteristics of the processed region

All variants of the processing parameters resulted in similar microhardness profile. This profile confirms with that found in earlier work conducted by Babu et al. (2008), Scialpi et al. (2007) on AA 6082, Rodrigues et al. (2009) on AA 6061, and Sato et al. (1999) on AA 6063. A typical example of microhardness measurement results is shown in Fig. 14, which corresponds to a sample processed at 850 rpm and 140 mm/min using two passes. In general, it can be seen that the SZ became much softer than that of the unaffected base metal. In addition, the TMAZ still experiences more softening than the SZ. The relatively high hardness of the base material in the as-received condition is due to the type of treatment being T651. In this treatment the material was solutionized, quenched, stress relieved then artificially aged for a prolonged period of time at temperature ~180 °C. Within the SZ, severe plastic deformation and friction heating during FSP result in generation of a recrystallized equiaxed microstructure due to the occurrence of DRX, which results in low dislocation density structure. The SZ softening with respect to the base metal is due to the decomposition of β″ precipitates, the coarsening of precipitates into semi-coherent and non-coherent equilibrium precipitates (over aged precipitate structure) and the low dislocation density associated with the dynamically recrystallized structure. Another probable reason is that intense deformation causes fragmentation of second phase particles and precipitates, as shown earlier, leading them to be redistributed in new locations at the interior of grains as reported by Dadbakhsh et al. (2010). This consequently leads to less strain and stress localization contributing to material softening.

The TMAZ exhibited significant softening when compared with the SZ. This has been noted on both the advancing and retreating sides as shown in Fig. 14. This softening can be attributed to the dissolution and growth of precipitates as concluded by Sato et al. (1999) during processing based on fact that the second phase particles exhibit less density and large particle size compared to SZ as shown in Fig. 10.

The influence of varying the number of passes and different traverse speeds on the SZ average hardness is shown in Fig. 15(a) and (b) respectively. Increasing the number of passes at constant traverse speed is accompanied by SZ softening. This softening is attributed to the larger grain size, as was shown above in Fig. 8(a), accompanying the increase of number of passes. The relation between hardness and grain size is in good agreement with previous work done by Nakata et al. (2006), who has correlated them using Hall–Petch

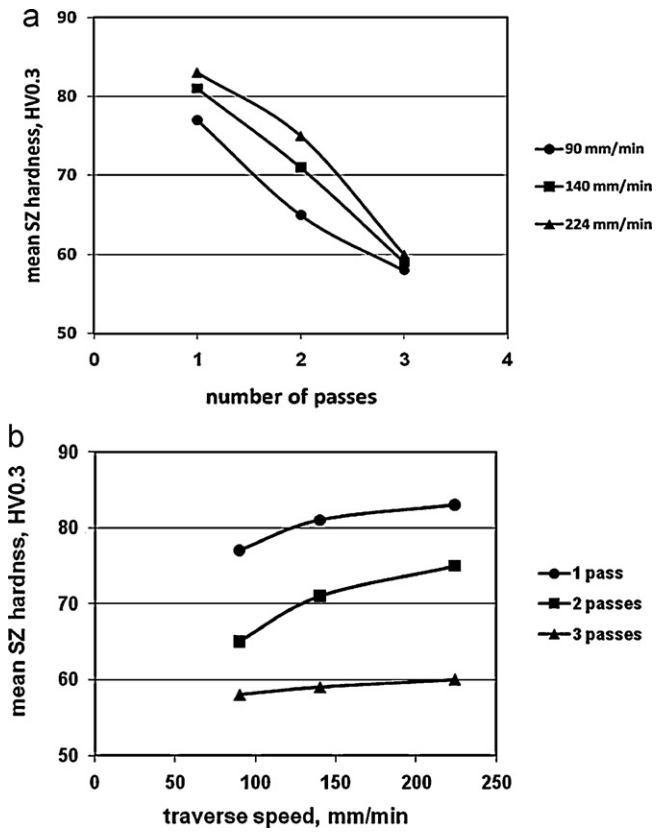

Fig. 15. The influence of varying: (a) the number of FSP passes; (b). traverse speed on the SZ mean hardness at.

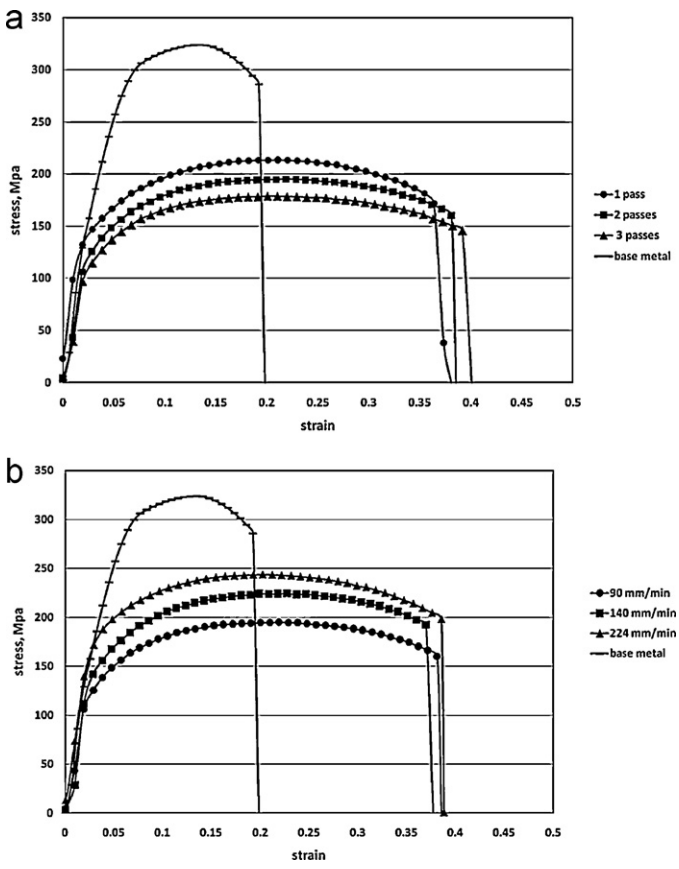

Fig. 16. Stress–strain behavior of the SZ showing the: (a) influence of varying the number of passes at 90 mm/min traverse speed; (b) influence of varying the traverse speed at 2 passes.

equation, which states that the hardness is inversely proportional to grain size.

Increasing the traverse speed on the other hand, at a given number of passes, increases the SZ hardness; however, this increase is slight with the three passes condition as shown in Fig. 15(b). Increasing the traverse speed results into higher stirring action of plasticized material, higher degree of deformation and also material flow leading to more nucleation sites of fine precipitates in which, localization of stress and strain accumulates at its boundaries.

In this respect, Dadbakhsh et al. (2010) reported that fine precipitates assist work hardening by pinning dislocations. The work hardening and the localization of stress and strain at the particles boundary increase the material hardness as well as reduce its ductility. This encourages the strain hardening of the deformed material and consequently the hardness of the SZ. Fig. 16 (a) and (b) shows the influence of varying the number of passes and the traverse speeds respectively on the stress–strain curves. In general, the ultimate tensile strength (UTS) and the strain at fracture within all specimens ranged within 178–244 MPa and 0.36–0.4 respectively. On the other hand, the base material in the as-received condition parallel to rolling direction gave higher strength; 323 MPa, and less strain at fracture; 0.2 indicating that FSP reduces strength and enhances ductility.

Fig. 17 summarizes the tensile test results of the SZ. Increasing the number of passes at a given traverse speed decreases the UTS of the SZ, as in Fig. 17a. Increasing the traverse speed on the other hand increases the UTS as shown in Fig. 17(b). These results are in good agreement with the hardness results.

The average hardness results of the SZ, which is related to β'' precipitate, is a reason for the reduction of the UTS when increasing the number of passes due to the softening of the SZ as shown

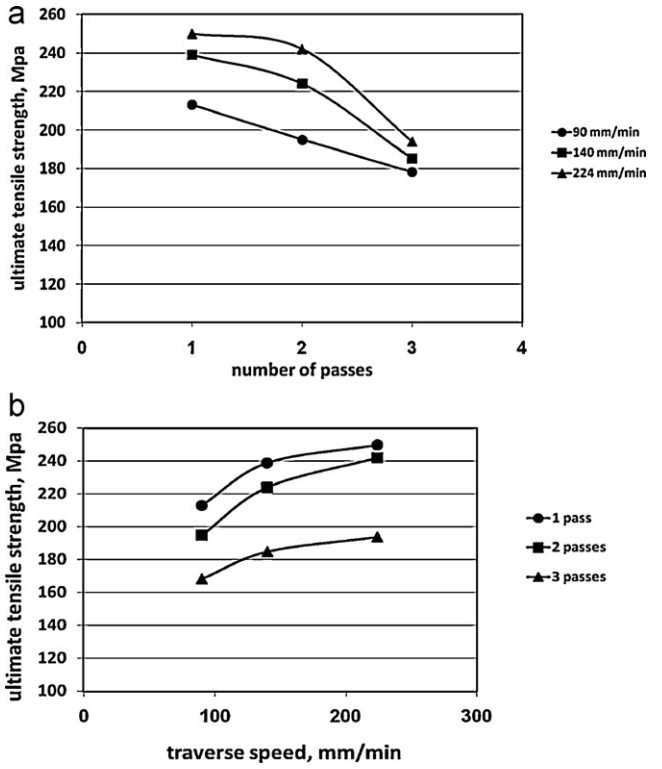

Fig. 17. The relation between the ultimate tensile strength of the SZ with: (a) number of passes; (b) traverse speeds.

in Fig. 17(a). Increasing the number of passes intensifies the deformation and fragmentation of precipitates as well as accumulates heat which promotes the decomposition of β″ precipitates, thus softening the material.

One of the reasons to this reduction is the increase in SZ grain size which is accompanied with the increased of number of passes. It is also suggested that the reduction of the UTS is due to the overaging effect which the subsequent passes cause to the previous one. Ma et al. (2006a) have suggested that when performing multiple-pass FSP, each subsequent FSP pass causes a short-term high temperature exposure of the previously processed zones, resulting in overaging of these zones. Therefore, the strength of the previously processed zones, which has undergone the maximum number of high-temperature thermal cycles, is lower than that of the subsequently processed zones.

Increasing the traverse speed on the other hand increases the UTS as shown in Fig. 17(b). This result can also be attributed to the presence of β″ precipitates. With low traverse speed; 90 mm/min, the specimen is subjected to relatively higher friction heating which promotes the dissolution of β″ precipitates thus reducing the UTS of the SZ.

The size of second phase particles/precipitates probably plays a role in the strength of the SZ. As shown earlier in Fig. 12(b) that increasing the traverse speed reduces the particles size. Hence, it can be stated that the smaller the particles size the higher the UTS. Dadbakhsh et al. (2010) have studied the same alloy type, and reported that these particles assist work hardening by pinning dislocations which consequently increases the accumulated strains thus increases the strength of material at the particle boundary [flow barrier]. This is normally more pronounced with smaller particle size than that with larger ones.

As it has been shown above that increasing the number of passes increases both the grain size and the particle area fraction whereas, it reduces the particle size. It is apparent from tensile test results that there is a good agreement between UTS and the hardness values as well as particle size, where the UTS increases with increasing hardness and reducing particle size. On the contrary, increasing the traverse speed did not affect the grain size; however, it reduced the particle size and increased the UTS. This again appears to indicate that the particle size and its corresponding area fraction play the major role in determining the UTS of SZ.

3.4. *Influence of tool rotational speed on the mechanical and microstructural characteristics of the SZ*

As depicted from Fig. 17(a) and (b), the highest UTS value obtained among all processing parameters correspond to single pass and traverse speed of 224 mm/min. In order to determine the influence of the tool rotational speed on the mechanical and microstructural characteristics of the SZ, two additional FSP runs were conducted using 1070 and 1350 rpm at traverse speed of 224 mm/min with a single pass. All literature have agreed upon that the tool rotation speed in FSW/FSP results in stirring and mixing of material around the rotating pin which in turn increase the temperature of the material as reported by Jayaraman et al. (2010) and also summarized by Mishra and Ma (2005). Increasing the tool rotational speed caused the SZ grains to grow, as shown in Fig. 18. This is due to the increased friction heating arising between the tool shoulder and pin with the processed material. It can therefore be stated that the tool rotational speed is more influential on the SZ mean grain size than the traverse speed does since its effect was marginal as seen in Fig. 8(b).

The influence of increasing the tool rotational speed on the particle area fraction; density, and mean particle size can be seen in Fig. 19(a) and (b) respectively. Increasing the rotational speed at constant traverse speed increases the stirring influence exerted by

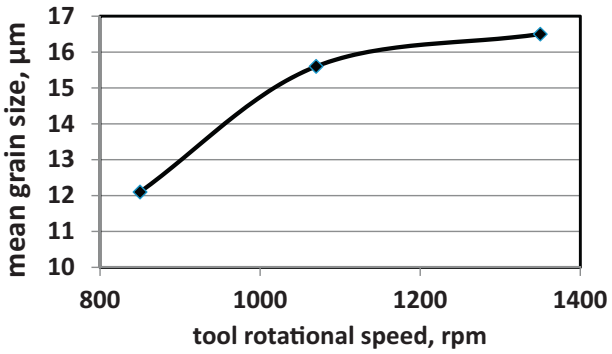

Fig. 18. The influence of tool rotational speed on the mean grain size of the SZ.

the tool on the plasticized SZ material. This promotes fragmentation of particles as well as re-precipitation of new particles thus occupying larger area; increases their density, with respect to the matrix as reported by Mironov et al. (2008). The fragmentation consequently causes more particle refinement, which is expressed in smaller particle diameter, as reported by Nakata et al. (2006) and observed in Fig. 19(b).

Fig. 20 shows the hardness distribution across the FSP'ed specimens at different tool rotational speeds. Similar to the hardness distribution shown earlier in Fig. 14, that the SZ became much softer than that of the unaffected base metal. In addition, the TMAZ still experiences more softening than the SZ. However, it can be noted that the hardness values of the SZ corresponding to 850 rpm [83 HV] are slightly higher than the other rotational speeds tested [78 HV]. This indicates that increasing the tool rotational speed has almost no substantial effect on the SZ hardness. This can be further seen

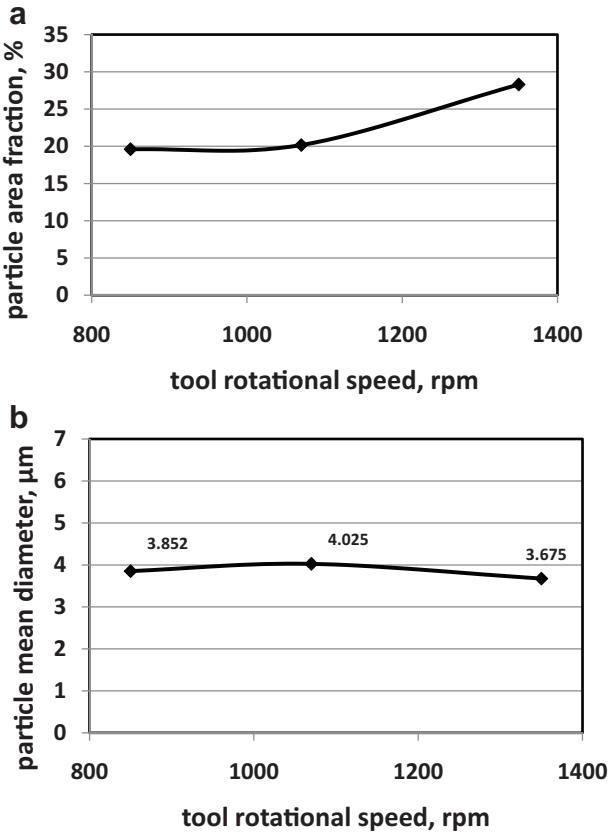

Fig. 19. Influence of tool rotational speed on: (a) particle area fraction; (b) particle mean diameter.

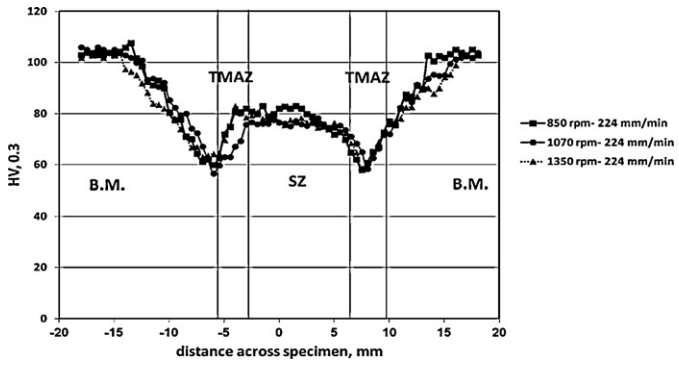

Fig. 20. Hardness distribution across FSP'ed specimen at different tool rotational speeds and constant traverse speed. *Note*: advancing side is on the right of SZ and the retreating side is on the left.

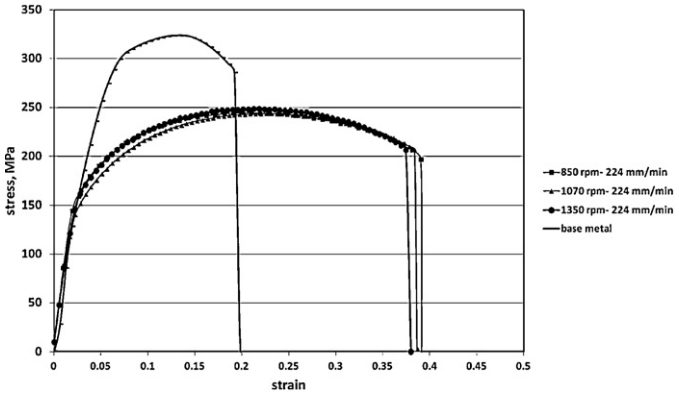

Fig. 21. Stress–strain curves of specimens FSP'ed at different tool rotational speeds and constant traverse speed.

in Fig. 21, which shows that increasing the rotational speed also did not have a significant influence on the stress–strain curves. The elastic and plastic parts of the stress–strain curves exactly overlap showing a good consistency of the mechanical properties of the tested specimens, thus indicating that varying the tool rotational speed had no effect on their UTS values.

4. Conclusions

FSP has been conducted on 6082-T651 Aluminum Alloy by applying one through three-100% overlapping passes and also three different traverse speeds. The following can be concluded:

1. The effect of increasing the number of passes led to an increase in the SZ-grain size, more dissolution and re-precipitation with simultaneous intense fragmentation of second phase particles all of which are attributed to accumulated thermal cycles.
2. Increasing the number of passes is accompanied by an increase in the average misorientation angle and fraction of HAGBs that are related to the extent of DRX.
3. The number of passes is more influential on the DRX of grain size of the SZ than the traverse speed does.
4. The particle size and particle area fraction within the SZ are inversely proportional.
5. Increasing the number of passes accumulates more heat leading to dissolution of hardening – β" phase which softens and reduces the UTS of the SZ.
6. Increasing the traverse speed reduces the second phase particle size, increases the mean hardness and UTS of the SZ.
7. The influence of increasing the tool rotational speed on the SZ mechanical properties as well as SZ hardness was insignificant whereas it caused grain coarsening in the SZ.

Acknowledgements

The authors would like to express their sincere thanks to the Center of Excellence for Research in Engineering Materials (CEREM) – College of Engineering – King Saud University, for supporting this work.

References

Adamowski, J., Szkodo, M., 2007. Friction stir welds (FSW) of aluminum alloy AW6082-T6. Journal of Achievements in Materials and Manufacturing Engineering 20 (January–February (1–2)), 403–406.
Babu, G., Raghu, Murti, K.G.K., Janardhana, G.R., 2008. An experimental study on the effect of welding parameters on mechanical and microstructural properties of AA 6082-T6 friction stir welded butt joints. ARPN Journal of Engineering and Applied Sciences 3 (October (5)).
Cabibbo, M., McQueen, H.J., Evangelista, E., Spigarelli, S., Di Paola, M., Falchero, A., 2007. Microstructure and mechanical property studies of AA 6056 friction stir welded plate. Materials Science and Engineering A 460–461, 86.
Dadbakhsh, S., Karimi Taheri, A., Smith, C.W., 2010. Strengthening study on 6082 Al alloy after combination of aging treatment and ECAP process. Materials Science and Engineering A 527, 4758–4766.
Elangovan, K., Balasubramanian, V., 2008. Influences of tool pin profile and tool shoulder diameter on the formation of friction stir processing zone in AA6061 Aluminum Alloy. Materials and Design 29, 362–373.
El-Danaf, E.A., E.L-Rayes, M.M., Soliman, M.S., 2010. Friction stir processing: an effective technique to refine grain structure and enhance ductility. Materials and Design 31, 1231–1236.
Frigaard, O., Grong, O., Midling, O.T., 2001. A process model for friction stir welding of age hardening aluminum alloys. Metallurgy and Materials Transactions A 32, 1189.
Fujda, M., Kvackaj, T., Nagyova, K., 2008. Improvement of mechanical properties for EN AW 6082 aluminium alloy using equal-channel angular pressing (ECAP) and post-ECAP aging. Journal of Metals, Materials and Minerals 18 (1), 81–87.
Johannes, L.B., Charit, I., Mishra, R.S., Verma, R., 2007. Enhanced superplasticity through friction stir processing in continuous cast AA5083 aluminum. Materials Science and Engineering A 464, 351–357.
Johannes, L.B., Mishra, R.S., 2007. Multiple passes of friction stir processing for the creation of superplastic 7075 aluminum. Materials Science and Engineering A 464, 255–260.
Jayaraman, M., Sivasubramanian, R., Balasubramanian, V., 2010. Establishing relationship between the base metal properties and friction stir welding process parameters of cast aluminium alloys. Materials and Design 31, 4567–4576.
Kamp, N., Sullivan, A., Tomasi, R., Robson, J.D., 2006. Modelling of heterogeneous precipitate distribution evolution during friction stir welding process. Acta Materialia 54, 2003–2014.
Kuijpers, N.C.W., Kool, W.H., Koenis, P.T.G., Nilsen, K.E., Todd, I., van der Zwaag, S., 2003. Assessment of different techniques for quantification of -Al(FeMn)Si and -AlFeSi intermetallics in AA 6xxx alloys. Materials Characterization 49, 409–420.
Kuijpers, N.C.W., Vermolen, F.J., Vuik, C., Koenis, P.T.G., Nilsen, K.E., Todd, I., van der Zwaag, S., 2005. The dependence of the -AlFeSi to -Al(FeMn)Si transformation kinetics in Al–Mg–Si alloys on the alloying elements. Material Science Engineering A 394 (1–2), 9–19.
Liu, F.C., Ma, Z.Y., 2008. Low-temperature superplasticity of friction stir processed Al–Zn–Mg–Cu alloy. Scripta Materialia 58, 667–670.
Ma, Z.Y., Sharma, S.R., Mishra, R.S., 2006a. Effect of multiple-pass friction stir processing on microstructure and tensile properties of a cast aluminum–silicon alloy. Scripta Materialia 54, 1623–1626.
Ma, Z.Y., Sharma, S.R., Mishra, R.S., 2006b. Effect of friction stir processing on the microstructure of cast A356 aluminum. Materials Science and Engineering A 433, 269–278.
McNelley, T.R., Swaminathan, S., Su, J.Q., 2008. Recrystallization mechanisms during friction stir welding/processing of aluminum alloys. Scripta Materialia 58, 349–354.
Miao, W.F., Laughlin, D.E., 1999. Precipitation hardening in aluminum alloy 6022. Scripta Materialia 40, 873–878.
Miao, W.F., Laughlin, D.E., 2000a. A differential scanning calorimetry study of aluminum alloy 6111 with different pre-aging treatments. Journal of Materials Science Letters 19, 201–203.
Miao, W.F., Laughlin, D.E., 2000b. Effects of Cu content and presaging on precipitation characteristics in aluminum alloy 6022. Metallurgy and Materials Transactions A 31, 361–371.
Mironov, S., Sato, Y.S., Kokawa, H., 2008. Microstructural evolution during friction stir-processing of pure iron. Acta Materialia 56, 2602–2614.
Mishra, R.S., Ma, Z.Y., 2005. Friction stir welding and processing. Materials Science and Engineering R 50, 1–78.

Mroczka, K., Pietras, A., 2009. FSW characterization of 6082 aluminum alloys sheets. Archives of Materials Science and Engineering 40 (December (2)), 104–109.
Murayama, M., Hono, K., Saga, M., Kikuchi, M., 1998. Atom probe studies on the early stages of precipitation in Al–Mg–Si alloys. Materials Science and Engineering. A 250, 127–132.
Murayama, M., Hono, K., 1999. Pre-precipitate clusters and precipitation processes in Al–Mg–Si alloys. Acta Materialia 47, 1537–1548.
Nakata, K., Kima, Y.G., Fujii, H., Tsumura, T., Komazaki, T., 2006. Improvement of mechanical properties of aluminum die casting alloy by multi-pass friction stir processing. Materials Science and Engineering A 437, 274–280.
Rodrigues, D.M., Loureiro, A., Leitao, C., Leal, R.M., Chaparro, B.M., Vilaça, P., 2009. Influence of friction stir welding parameters on the microstructural and mechanical properties of AA 6016-T4 thin welds. Materials and Design 30 (6), 1913–1921.
Scialpi, A., De Filippis, L.A.C., Cavaliere, P., 2007. Influence of shoulder geometry on microstructure and mechanical properties of friction stir welded 6082 aluminum alloy. Materials and Design 28, 1124–1129.
Sha, G., O'Reilly, K., Cantor, B., Titchmarsh, J.M., Hamerton, R.G., 2003. Quasi-peritectic solidification reactions in 6xxx series wrought Al alloys. Acta Materialia 51 (18), 1883–1897.
Takeda, M., Ohkubo, F., Shirai, T., Fukui, K., 1998. Stability of metastable phases and microstructures in the ageing process of Al–Mg–Si ternary alloys. Journal of Materials Science 33, 2385–2390.
Sauvage, X., Dïede, A., Cabello, A., Muñoz Huneau, B., 2008. Precipitate stability and recrystallisation in the weld nuggets of friction stir welded Al–Mg–Si and Al–Mg–Sc alloys. Materials Science and Engineering A 491, 364–371.
Sato, Y.S., Kokawa, H., Enomoto, M., Jodan, S., 1999. Microstructural evolution of 6063 aluminum during friction stir welding. Metallurgical and Materials Transactions A 30A (September), 2429–2437.
Urreta, S.E., Louchet, F., Ghilarducci, A., 2001. Fracture behavior of an Al–Mg–Si industrial alloy. Materials Science and Engineering A 302, 300–307.
Woo, W., Choo, H., Brown, D.W., Feng, Z., 2007. Influence of the tool pin and shoulder on microstructure and natural aging kinetics in a friction-stir-processed 6061-T6 aluminum alloy. Metallurgical and Materials Transactions A 38A (January), 69–76.